Dissipation induced instabilities of structures coupled to a flow

Olivier Doaré
IMSIA, ENSTA ParisTech, CNRS, CEA, EDF, Université Paris-Saclay, 828 bd des Maréchaux, 91762 Palaiseau cedex France

In these lecture notes, we are concerned with the instabilities to which are subjected some structures when they are coupled to a flow. These instability phenomena are very common, they can be observed in many engineering domains as in aeronautics, where wings or panels can bear strong deformations in flows at large velocities (Theodorsen, 1979), maritime engineering, where long cables, risers, or slender towed structures may oscillate (Païdoussis, 2004; Païdoussis et al., 2011), nuclear industry, where one designs structures in the core and heat exchangers to prevent unwanted vibrations (Guo and Paidoussis, 2000), civil engineering, where some bridges may be prone to strong oscillations (Païdoussis et al., 2011), as proven by the famous accident of the Takoma-Narrows bridge (Billah and Scanlan, 1991). Instabilities due to fluid-structure couplings is also a natural phenomenon observed on plants (De Langre, 2008; Gosselin and Langre, 2009).

The manifestation of these instabilities are hence numerous and can be due to different coupling mechanisms. In a first part of these lecture notes, a review of the different instability mechanisms will be done.

A particular attention will be given to the influence of dissipation on the stability. It can be observed that some of these instabilities can be triggered earlier when dissipation is added to the system. This phenomenon may seem counter-intuitive from the point of view of someone working in structural mechanics. The phenomenon is however very common in fluid-structure interaction but also in systems involving gyroscopic forces. In the second part we will address the main features of such phenomena in two simple and representative systems: the two degrees of freedom airfoil and the fluid-conveying pipe.

Because of the eventual dammage they could cause, most of the research effort has been put on the prediction of these instability in order to prevent their apparition. Recently these instabilities have seen a renewed interest in the context of energy harvesting from flows (Allen and Smits, 2001; Taylor et al., 2001; Tang and Païdoussis, 2009; Barrero-Gil et al., 2010; Doaré and

Michelin, 2011). This leads us to consider the opposite objective. In the third part of this chapter, the basic principles of energy harvesting from flow-induced instabilities will then be presented.

1 Dynamics and instabilities of structures coupled to a flow

The analysis of a system coupling a flow and a compliant structure involves two complex physical domains, the fluid and solid domains, and their interaction at their common boundary. The later can be additionnally moving, leading to even more complexity. There is active research aiming at developing efficient computational methods in a general case of a large deformations of a solid in a turbulent flow (Bazilevs et al., 2013). In the present lectures, we pursue a different objective. We indeed want to evidence the fundamental instability phenomena and their sensibility to damping. For that purpose we only need to consider the properties of the equilibrium positions of the strucutre in the context of small perturbations in the fluid and the induced efforts on the structure.

Two fundamental systems will serve as model systems in the following:

- A rigid body mounted on springs, such that its rigid body dynamics is characterized by one or two degrees of freedom.
- A compliant panel or a compliant pipe, modelled as a beam or plate, interacting with an axial flow.

With these two systems we will be able to cover most of the fundamental flow-induced instability phenomena one may encounter.

1.1 Cross-flow instabilities

Rigid-body models In Figure 1a and 1c are shown two typical structures in presence of flow. These are slender structures whose axis of slenderness is perpendicular to the flow. From this propery these problems derive their name "cross flow" problems. The first example of Figure 1 consists of a wing oscillating along a given mode of deformation – here a first beam-like mode. An equivalent simplified problem consists of a 2D profile at a median position on the wing oscillating perpendicularly to a 2D-flow at the same velocity. This approximation becomes questionnable as soon as the profile geometry varies a lot along the span or boundary effects at the clamp or the free end of the wing introduce significant variations of the fluid forces. However, this modeling is able to capture most of the coupling physical phenomena occuring in its 3D counterpart.

The second example is a beam or cable that can oscillate in two directions. Its equivalent 2D simplified model is represented by a 2D profile

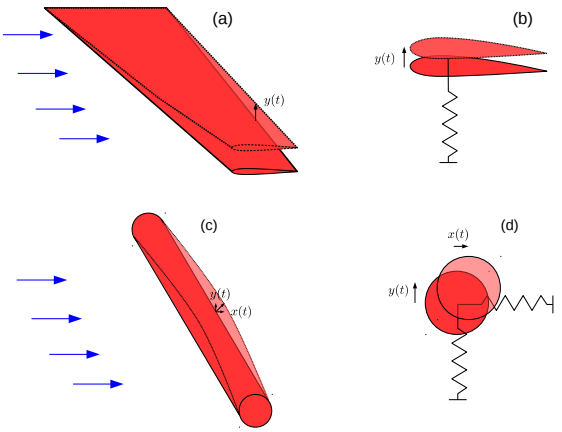

Figure 1. Examples of real structures in flows (left) and their equivalent 2D simplified models (right).

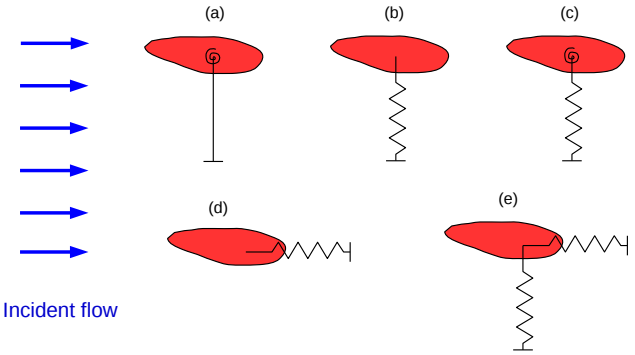

Figure 2. Five different generic models of oscillating rigid bodies in flows. (a) one DOF oscillator rotating around the elastic center E, (b) one degree of freedom (DOF) oscillator translating perpendicularly to the flow, (c) two DOFs oscillators having translation perpendicularly to the flow and rotation around the elastic center E, (d) one DOF oscillator translating along the flow direction, (e) two DOFs oscillator having translations alongside and perpendicularly to the incident flow.

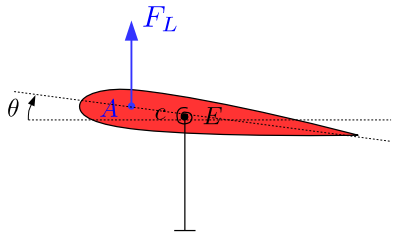

Figure 3. Schematic view of a wing profile in a flow, mounted on a torsionnal spring.

having the same shape as the cross-section of the structure, whose displacements are constrained by the presence of springs. The stiffnesses of the later model the modal stiffnesses of the structure along two particular modes. Here again, this simplification makes sense if we are interested in the main flow-structure physical phenomena arising in this configuration.

In Figure 2 is represented a tentative of an exaustive set of 2D rigid-body models of any cross section. These are one or two degrees of freedom (DOF) systems, involving three kinds of stiffnesses: a beam-like stiffness for a displacement perpendicular to the flow (cases b, c, e), a beam-like stiffness for a displacement in the the same direction as the flow (cases d,e) or a beam-like stiffness for a torsional deformation (cases a, c). These five examples allow to cover most of the encountered cross-flow-induced instabilities that will be evidenced hereafter.

Buckling instability due to negative flow-induced stiffness We consider first the case sketched in Figure 2a. It presented with more details on Figure 3 in the case of a 2D wing profile. The later is secured to the ground via a torsionnal spring of stiffness c, at the point E on the profile, referred to as the elastic center. The moment of inertia around the point E is noted J. The flow pressure distribution around the airfoil induces a force on the profile. This force is decomposed into a drag force F_D, in the direction of flow, and a lift force F_L, perpendicular to the flow. It is exerted at the aerodynamic center A, which is the reference point where the resultant force created by the aerodynamic pressure exert no moment on the solid. The angle of attack is noted θ, and the reference $\theta = 0$ is chosen such that it corresponds to the static equilibrium of the system when the flow velocity equals zero. The distance AE is noted d, counted positive when A is upstream the elastic center E.

For small variations of θ, the lift force contributes to a moment dF_L and the contribution of the drag force can be neglected, so that the dynamic equilibrium equation governing small variations of the angle of attack is:

$$J\ddot{\theta} + c\theta = dF_L. \tag{1}$$

We now make the three following asumptions:

- The lift force can be determined only through the knowlegde of the lift coefficient C_L,
$$F_L = \frac{1}{2}\rho U^2 S C_L, \tag{2}$$
where ρ is the density of the fluid, S is the equivalent surface of the object, its chord length times its spanwise length. This is a good approximation for large Reynolds numbers, and if it does not vary too much in the range of considered velocities.
- The velocity of the fluid-solid boundary remains small compared to the velocity of the fluid. The dynamics of the fluid hence occurs on small timescales compared to the solid dynamics. One can then consider that the lift coefficient, which is a consequence of the fluid dynamics, depends only on the solid's position θ.
- Small angle of attack variations are considered, hence the lift coefficient can be approached by $C_L \sim \theta\, \partial C_L/\partial\theta$. In the following, we note $C'_L = \partial C_L/\partial\theta$.

Equation (1) then writes,

$$J\ddot{\theta} + \left[k - \frac{1}{2}\rho U^2 S d C'_L\right]\theta = 0. \tag{3}$$

The influence of the fluid can hence be summarized as an added stiffness, whose sign depends on the sign of C'_L and d. Consider for instance the classical case of a thin aerodynamic profile, where $C'_L \simeq 2\pi$ (Dowell et al., 1995). The sign of the added stiffness is only determined by the position of the elastic center with respect to the aerodynamic center. If the former is upstream the aerodynamic center, $d > 0$, the added stiffness is positive and the presence of flow induces an increase of the system's natural frequency. Conversely, if the elastic center is downstream, $d < 0$, the added stiffness is negative, and the total stiffness vanishes when the flow velocity reaches the critical velocity,

$$U_b = \sqrt{\frac{2k}{\rho S d C'_L}}. \tag{4}$$

Above this limit value, the equilibrium position $\theta = 0$ is unstable and any perturbation is exponentially amplified with time until the profile reaches a

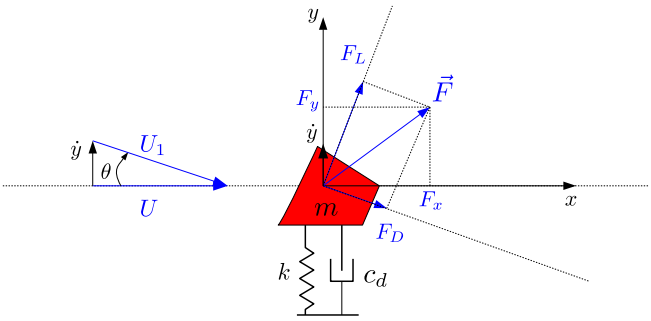

Figure 4. Sketch of a profile of any shape moving perpendicularly to the flow.

new equilibrium position. This instabillity is referred to as buckling instability.

1.2 Dynamic instability by negative flow-induced damping

The den Artog criterion Let us now consider the case sketched in Figure 2b. The profile displacement is now a translation perpendicular to the flow direction, noted y. A more detailed sketch of the system of interest is provided in Figure 4. The mass of the solid is m, and the stiffness of the spring is k. There is also a damping acting on the structure dynamics, modeled by a linear damping coefficient c_d. If the same asumptions as in the previous case are made, it is not possible to show that the fluid forces have any influence on the dynamics, because they do not depend on y. We now raise the hypothesis that the velocity of the fluid-solid boundary is negligible compared to the velocity of the fluid, and consider instead that from the point of view ot the flow, the solid is driven by a constant vertical translation speed $\dot{y}$. In the reference axis of the moving solid, the flow seen by the solid is now at the velocity

$$U_1 = \sqrt{U^2 + \dot{y}^2} \sim U, \tag{5}$$

and the angle of attack

$$\theta = \arctan\left(-\frac{\dot{y}}{U}\right) \sim -\frac{\dot{y}}{U}. \tag{6}$$

Provided $\dot{y}$ is not small compared to U, but $\dot{y}^2$ is small compared to U^2, the force coefficient in the vertical direction C_y can be approximated by

$$C_y \sim \theta \frac{\partial C_y}{\partial \theta} \sim -\frac{\dot{y}}{U} \frac{\partial}{\partial \theta} \left(C_L \cos\theta + C_D \sin\theta \right) \sim -\frac{\dot{y}}{U} \left(C'_L + C_D \right). \quad (7)$$

Inserting the resulting force in the dynamical oscillator equation, one obtains the following:

$$m\ddot{y} + \left[c_d + \frac{1}{2}\rho U S (C'_L + C_D) \right] \dot{y} + ky = 0. \quad (8)$$

The flow influence takes hence the form of an added damping. Its sign is the same as the sign of $C'_L + C_D$. If the later is positive, the consequence is a positive added damping. If it is negative, the system can present exponentially growing oscillations once the flow velocity is greater than

$$U_g = -\frac{2c_d}{\rho U S (C'_L + C_D)}. \quad (9)$$

This instability is generally referred to as *galloping*. The criterion for instability is called the *Den Artog* criterion (Blevins, 1990).

Drag crisis instability We now consider the case of a structural displacement in the direction of the flow, as sketched in Figure 2d. The dynamical equations governing the displacement x of the profile is

$$m\ddot{x} + c\dot{x} + kx = F_D, \quad (10)$$

where the drag force F_D reads

$$F_D = -\frac{1}{2}\rho (U + \dot{x})^2 S C_D \left(R_{Ec} \right), \quad (11)$$

S being the characteristic section offered to the flow. R_{Ec} is the equivalent Reynolds number in the referential of the moving solid,

$$R_{Ec} = \frac{(U + \dot{x})L}{\nu}, \quad (12)$$

with ν the kinematic viscosity of the fluid. Considering that $\dot{x} \ll U$, the drag force can be expressed at first order as,

$$F_D = -\frac{1}{2}\rho U^2 S \left(C_D(R_E) + 2\frac{\dot{x}}{U} C_D(R_E) + \frac{\dot{x}}{U} R_E \frac{\partial C_D}{\partial R_E} \right). \quad (13)$$

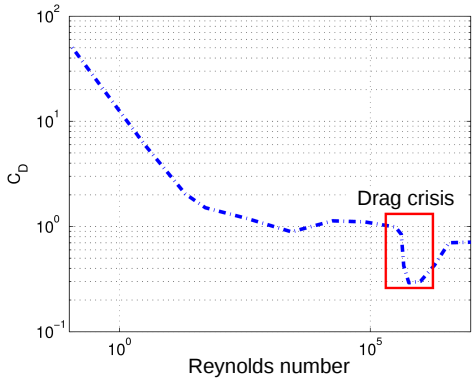

Figure 5. Drag coefficient of a rigid cylinder in cross flow as function of the Reynolds number. Drag crisis occurs between $R_E = 10^5$ and $R_E = 10^6$.

The flow hence induces an added damping which can be negative if,

$$2C_D(R_E) + R_E \frac{\partial C_D}{\partial R_E} < 0. \tag{14}$$

If the later condition is statisfied and if the induced negative damping has a greater amplitude than the structural damping c, a galloping type instability can occur.

For circular profiles, condition (14) is true in a particular range of Reynolds numbers, as represented in Figure 5. This phenomenon is called *drag crisis* and the associated instability is called *drag crisis* instability.

1.3 Wing instabilities due to mode coupling

The case of a two degrees of freedom profile that can translate and rotate around the elastic center is now considered. This case corresponds to the generic configuration of Figure 2c, and is sketched with more details in the case of a thin wing profile in Figure 6. The general case where the aerodynamic center A, the elastic center E and the center of gravity G are three distinct points is considered. As in section 1.1, we consider that the solid's velocity is negligible compared to the flow velocity, such that the aerodynamic efforts depend only on the solid's position. The dynamical

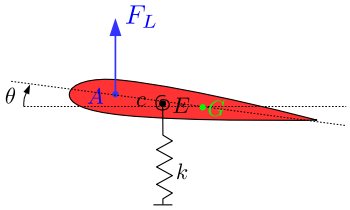

Figure 6. Schematic view of a wing profile in a flow, mounted on a spring and a torsionnal spring, modeling the dynamics of a wing whose deformation can be along torsional and a flexural modes.

equations governing small variations of y and θ read then

$$m\ddot{y} + ky + kx\theta = F_L, \tag{15}$$

$$J\ddot{\theta} + (c + kx^2)\theta + kxy = (x + d)F_L, \tag{16}$$

where x is the distance GE, counted positively when the center of gravity is downstream the elastic center. In the context of small perturbations, the lift coefficient is again approximated by $\theta C'_L$ and the dynamical system (15-16) writes

$$\begin{bmatrix} m & 0 \\ 0 & J \end{bmatrix} \begin{bmatrix} \ddot{y} \\ \ddot{\theta} \end{bmatrix} + \begin{bmatrix} k & kx - \frac{1}{2}\rho U^2 S C'_L \\ kx & c + kx^2 - \frac{1}{2}\rho U^2 S d C'_L \end{bmatrix} \begin{bmatrix} y \\ \theta \end{bmatrix} = \begin{bmatrix} 0 \\ 0 \end{bmatrix}. \tag{17}$$

It can be written in the following classical form,

$$M\vec{\ddot{q}} + K\vec{q} = 0, \tag{18}$$

where M is referred to as the mass matrix, K the stiffness matrix and $\vec{q}$ the state vector. Flow forces appear then in the stiffness matrix in the form of one diagonal term and one off-diagonal term. Both terms can be positive or negative, depending on the sign of d and C'_L. This equations set has a similar form as the classical equations derived by Ziegler in 1952 (Ziegler, 1952) in the case of a double pendulum submitted to a follower force. This case is treated in details in the chapter written by Davide Bigoni. In the the present airfoil model the flow couples flexural and torsional wing modes whereas in the double pendulum a follower force couples the two rotation angles of the pendulum.

Looking for harmonic solutions of this system in the form $[y, \theta]^t = \vec{V}\mathrm{e}^{-\mathrm{i}\omega t}$, one obtains the following eigenvalue problem,

$$M^{-1}K\vec{V} = \omega^2\vec{V}. \tag{19}$$

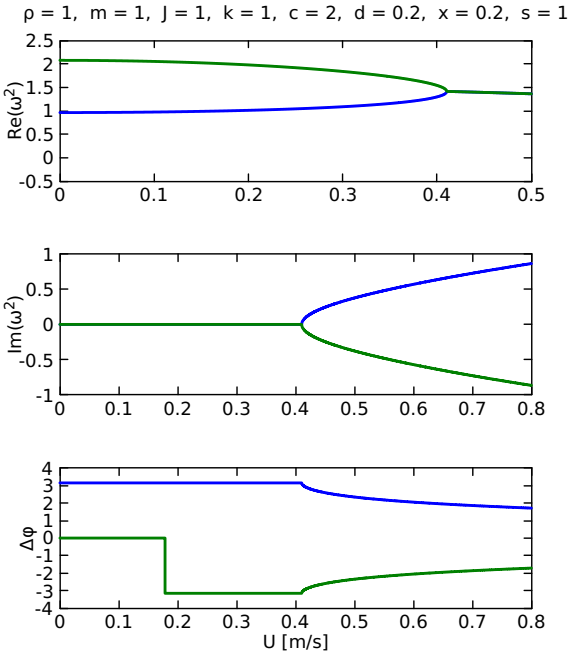

Figure 7. Evolution of ω^2 as function of the flow velocity U. Typical values of the parameters are chosen. Third plot: phase difference betwwen rotational and translational modal components.

If $U = 0$, one can easily observe that the resolution of this problem consists of calculating the eigenvalues of a symmetric positive definite matrix. Hence, in absence of flow ω^2 is real and positive. The eigenfrequencies are real, and the solution of the problem hence takes the form of undamped oscillations. If $U \neq 0$, the matrix $M^{-1}K$ is not symmetric anymore and the eigenvalues may be positive, negative or complex. An example of the evolution of the eigenfrequencies of this system is presented on Figure 7. At $U = 0$, the square of the two eigenfrequencies are real and positive. In a general case where E and G are not the same, the associated modes (eigenvectors) couple movements of rotation and translation. When the velocity is increased, the two eigenfrequencies approach until they become equal at a critical velocity $U_f \sim 0.41$. Above this velocity, the eigenfrequencies of the system form complex conjugate pairs. The dynamics associated to one eigenfrequency

and its corresponding eigenvector reads,

$$\begin{bmatrix} y \\ \theta \end{bmatrix} = \mathrm{e}^{\omega_\mathrm{i} t} \left(\vec{V} \mathrm{e}^{-\mathrm{i}\omega_\mathrm{r} t} \right), \tag{20}$$

where $\vec{V}$ is the eigenvector associated to the eigenvalue ω^2 and the subscripts r and i refer to the real and imaginary parts respectively. In equation (20), one regognizes an oscillation at the frequency ω_r whose amplitude varies as $\mathrm{e}^{\omega_\mathrm{i} t}$. Hence, a positive imaginary part of the eigenfrequency indicates an instability. The amplitude of the oscillations grows exponentially with time, until eventually non linear effects not taken into account in the present model saturate this growth phenomenon.

This instability arises when two structural modes are coupled by the flow in the stiffness matrix if this coupling is skew-symmetric. It is hence referred to as *coupled mode flutter*. It is also sometimes called *frequency coalescence instability* because theoretically and experimentally, it is preceded by a rapprochement of two eigenfrequencies.

In the third plot Figure 7 the phase difference between the rotation component and the translation component of the eigenvetor is plotted for the two modes as function of the flow velocity. Below the critical velocity, the phase difference equals zero or π. Hence translation and rotation are in phase or in phase opposition. Above the critical value we see that the phase varies slowly. The unstable eigenmode has a corresponding positive phase difference, while the damped mode has a negative phase difference. In order to get insight on the link between the phase and the instability, let us analyse the energy transfers between the flow and the structure by comparing the work done by the lift force on the system on both modes: the temporally amplified mode and the temporally damped mode. The kinematics of the system along these two modes is given by the real part of equation (20). It its sketched in Figure 8. In case (a), the airfoil oscillates along a mode that is temporally amplified. It can be observed on this figure that the lift force F_p and the velocity of the profile $\dot{y}$ are in the same direction. The work done by the fluid on the structure is hence positive if integrated on a period. Conversely, for a damped mode, the work done by the flow on the structure is negative. In case (a), the rotation θ is ahead of phase compared to the displacement y, while in case (b), it is lagging behind. This is in agreement with the phase plot in Figure 7.

1.4 Axial flow problems

In section 1.1, focus has been put on slender structures coupled to a flow in a direction perpendicular to its slenderness direction. This was

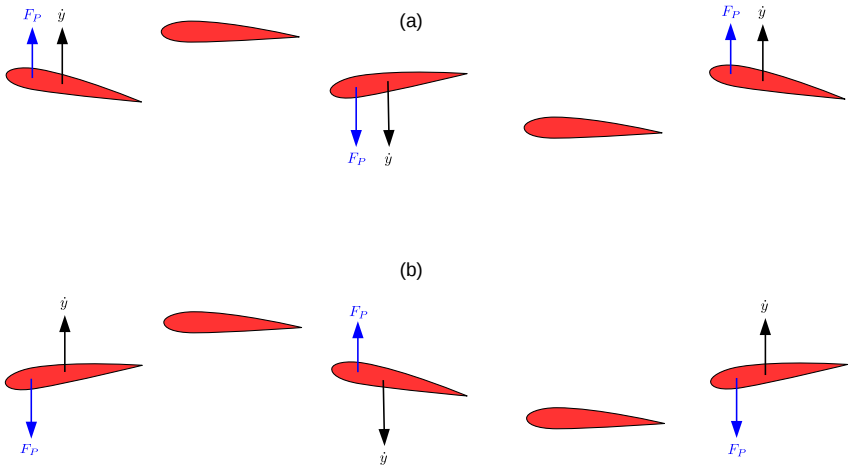

Figure 8. Typical kinematics of the airfoil when oscillating along an unstable mode (a) and a stable mode (b).

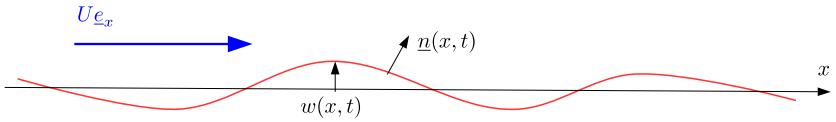

Figure 9. Sketch view of a fluid-solid interface. Locally, it consists of a wall which is plane when unperturbed, below a flow at the velocity U aligned with the wall.

molelled considering discrete structures coupled to a 2D-flow. The aerodynamic effects have been described only through the knowledge of lift and drag coefficients, which eventually depend on the discrete kinematic variables and the Reynolds number. We want now to address another generic case which consist of a compliant slender structure interacting with a flow in the direction of the slenderness.

Flow effects on a moving boundary As a first approach we will consider the deformation of a simple surface in contact of a potential and irrotationnal flow. We will show that the flow can induce added inertia, damping and stiffness.

Consider the system represented in Figure 9. It consists of a compliant

boundary that locally deforms below a potential and irrotationnal flow. The velocity and pressure fields in the flow are $\underline{U}$ and P respectively. In the reference configuration where the boundary is undeformed, it is plane and the fluid has locally an homogeneous and constant flow velocity $U_0\underline{e}_x$. Consider a solid's displacement of small amplitude of the form,

$$\underline{w} = \varepsilon w \underline{e}_y, \tag{21}$$

where $\varepsilon \ll 1$ is a small amplitude parameter. At the fluid-solid interface, the normal velocity of the fluid has to be equal to the normal velocity of the solid,

$$\underline{U}.\underline{n} = \frac{\partial \underline{w}}{\partial t}.\underline{n} \tag{22}$$

Each quantity in this boundary condition may be decomposed as a Taylor expansion at order one,

$$\underline{n} = \underline{e}_y - \varepsilon \frac{\partial w}{\partial x}\underline{e}_x, \tag{23}$$

$$\underline{U} = U_0\underline{e}_x + \varepsilon \underline{u}, \tag{24}$$

$$\frac{\partial \underline{w}}{\partial t} = \varepsilon \frac{\partial w}{\partial t}\underline{e}_y. \tag{25}$$

At order zero, the kinematic boundary condition $U_0(\underline{e}_x.\underline{e}_y) = 0$ is readily satisfied, while at order one, it takes the following form,

$$\underline{u}.\underline{e}_y = \frac{\partial w}{\partial t} + U_0 \frac{\partial w}{\partial x}, \tag{26}$$

which is also known as the impermeability condition (Païdoussis, 2004). The velocity potential Ψ is now introduced,

$$\underline{\text{grad}}\, \Psi = \underline{U}. \tag{27}$$

The later may be also decomposed between a stationnary part and a fluctuation of small amplitude,

$$\Psi = U_0 x + \varepsilon \psi, \tag{28}$$

with

$$\underline{\text{grad}}\, \psi = \underline{u}. \tag{29}$$

Introducing (29) in the incompressibility condition $\text{div}\underline{u} = 0$, we show that the velocity potential satisfies a Laplace equation,

$$\Delta \psi = 0, \tag{30}$$

with the following boundary equation:

$$\frac{\partial \psi}{\partial y} = \frac{\partial w}{\partial t} + U_0 \frac{\partial w}{\partial x}. \tag{31}$$

We now make use of the momentum conservation equation for an inviscid and incompressible flow,

$$\rho \frac{\partial \underline{U}}{\partial t} + \left(\underline{\underline{\text{grad}}}.\underline{U} \right) \underline{U} + \underline{\text{grad}} P = 0. \tag{32}$$

At order zero, this equation becomes,

$$\rho \, \underline{\text{grad}} \left(U_0 \, \underline{e}_x \, . \, \underline{\text{grad}} \psi_0 \right) + \underline{\text{grad}} p_0 = 0. \tag{33}$$

After integrating with respect to space, this law reads,

$$\frac{1}{2} \rho \, U_0^2 + p_0 = \text{ct}, \tag{34}$$

ct being an integration constant. This is the Bernoulli equation satisfied by the permanent quantities of the flow. In our particular case of an homogeneous flow, this is readiliy satisfied since both velocity and pressure are constant in the whole fluid domain.

At order one, the momentum conservation law can then be expressed in the following form,

$$\rho \, \underline{\text{grad}} \frac{\partial \psi}{\partial t} + \rho \, \underline{\text{grad}} \left(U_0 \, \underline{e}_x \, . \, \underline{\text{grad}} \psi \right) + \underline{\text{grad}} \, p = 0. \tag{35}$$

The later expression can be integrated with respect to space, which leads to the unsteady Bernoulli equation,

$$p = -\rho \frac{\partial \psi}{\partial t} - \rho U_0 \frac{\partial \psi}{\partial x}. \tag{36}$$

This equation links the pressure in the fluid to the velocity potential. It has to be noted that no integration constant has been kept here, since we are only dealing with the fluctuations. We are then faced to a Laplace problem for the velocity potential (30) with the boundary condition (31). Once the potential ψ is obtained for a prescribed displacement, the pressure is calculated using the instationnary Bernoulli equation (36).

Let us consider a displacement as the product of a time and space functions,

$$w(x,t) = q(t)\phi(x). \tag{37}$$

Thanks to the linearity of the fluid-solid problem, the solution for the velocity potential is looked for as a sum of two contributions,

$$\psi = U_0\psi_1 + \psi_2, \tag{38}$$

ψ_1 and ψ_2 satisfying the Laplace equation, with the following boundary conditions,

$$\frac{\partial\psi_1}{\partial y} = \frac{\partial w}{\partial x}\,, \quad \frac{\partial\psi_2}{\partial y} = \frac{\partial w}{\partial t}. \tag{39}$$

The form of the boundary conditions indicates that ψ_1 and ψ_2 can be choosen of the form,

$$\psi_1 = q(t)\varphi_1(x)\,, \quad \psi_2 = \frac{\partial q(t)}{\partial t}\varphi_2(x). \tag{40}$$

Finally, after applying the unsteady Bernoulli equation (36) on the potential (38), the pressure is found in the form of the sum of terms proportional to the acceleration, the velocity and the displacement of the fluid-solid interface,

$$p = -\rho\varphi_2\ddot{q} - \rho U_0\left(\varphi_1 + \frac{\partial\varphi_2}{\partial x}\right)\dot{q} - \rho U_0^2\varphi_1 q. \tag{41}$$

The pressure in the fluid appears as the sum of three contributions, whose time dependence are respectively proportional to the acceleration, the velocity and the displacement of the plate. Hence, once eventually projected on the solid's displacement these terms will induce added mass, damping and stiffness.

When the kinematics is decomposed along several modes ϕ_n, $n = 1...N$, the linearity of the fluid problem allows to decompose the pressure perturbation in the fluid on pressure modes p_n, $N = 1...N$. Each pressure mode may exert a forcing on each displacement mode. As a consequence, the flow will couple the different modes of the structure through stiffness, damping and inertia terms.

Slender structures in presence of axial flow The general deformation introduced in section 1.4 can be sought as a local deformation of the interface of any compliant solid. From now on, we will focus on this particular geometry, which is representative of a large number of systems, for instance plates, flags, cylinders in axial flows, pipes with internal flows. Two examples will be treated: a vibrating plate with a flow on one side (Figure 10a) and a pipe conveying fluid (Figure 10b). For these two systems we make the asumption that the solid part is a slender beam or plate subjected to a

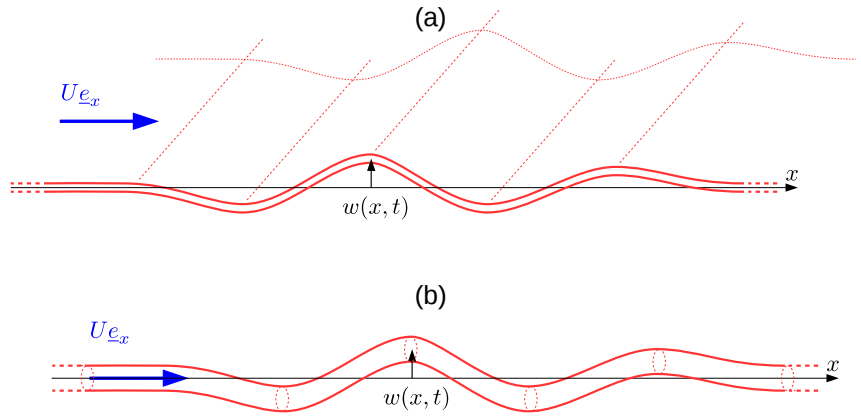

Figure 10. Slender structures interacting with an axial flow. (a) Infinite span plate below an inviscid and irrotationnal flow at velocity U. (b) Pipe conveying fluid.

transversal deflection $w(x)$ of small amplitude, such that it can be modeled under the Euler-Bernoulli beam approximation,

$$B\frac{\partial^4 w}{\partial x^4} + m\frac{\partial^2 w}{\partial t^2} = f(x,t), \quad + \text{boundary conditions.} \tag{42}$$

For the plate sketched in Figure 10a, B is the flexural rigidity of a plate of thickness h, made of a material of Young's modulus E and Poisson's coefficient ν, $B = Eh^3/(1-\nu^2)$, m is the surface density of the plate and $f(x,t)$ is the opposite of the fluid pressure at $y = 0$:

$$f = -p(x, y = 0, t). \tag{43}$$

For the fluid-conveying pipe sketched in Figure 10b, B is the flexural rigidity of a beam of annular cross section (Blevins, 1990) and m is the lineic density of this beam. The righthand term $f(x,t)$ is now a force per unit length which reads,

$$f = \int_\Gamma -p\underline{n}.\underline{e}_y \mathrm{d}L, \tag{44}$$

where Γ is the fluid-solid boundary at x, represented by a closed line, and $\underline{n}$ is the unitary vector normal to the boundary, directed from the solid to the fluid. For a pipe of circular section of radius R, Γ would be the circle of radius R, centered a $(x, y = 0, z = 0)$.

Dispersion relation The study of stability properties of slender structures like beams and plates is first performed with respect to the waves propagating in such structures. Considering a disturbance in the form of a plane harmonic wave

$$w = w_0 \mathrm{e}^{\mathrm{i}(kx-\omega t)}, \tag{45}$$

solving the Laplace problem (30) for the velocity potential with boundary condition (31) and using the unsteady Bernoulli equation (36) gives the pressure in the fluid generated by the solid's perturbation,

$$p = \frac{w_0}{|k|}(\omega - Uk)^2 \mathrm{e}^{-|k|y} \mathrm{e}^{\mathrm{i}(kx-\omega t)}. \tag{46}$$

The fluid-solid force f in equation (42) is then $f = -p(x, y = 0, t)$. Inserting this force and the displacement in the form of the harmonic plane wave in equation (42) leads to the dispersion relation, an algebraic equation that links the wavenumber k to the frequency ω,

$$D(k, \omega) = Dk^4 - m\omega^2 - \frac{\rho}{|k|}(\omega - Uk)^2 = 0. \tag{47}$$

The same calculation can be performed in the case of the circular geometry of the fluid-conveying pipe, where the same fluid equations are satisfied, with the same kind of boundary conditions, but on an interface of different geometry (Γ contour of equation 44). Solving this equation leads to the following expression for the pressure in the fluid domain,

$$p = \rho(\omega - Uk)^2 \frac{2I_1(kr)}{k[I_0(kR) + I_2(kR)]} \sin\theta \mathrm{e}^{\mathrm{i}(kx-\omega t)}. \tag{48}$$

Using equation (44), we obtain the following expression for f,

$$f = \rho(\omega - Uk)^2 \frac{2\pi R I_1(kR)}{k[I_0(kR) + I_2(kR)]} w_0 \mathrm{e}^{\mathrm{i}(kx-\omega t)}, \tag{49}$$

which takes the following form if the wavelength is large compared to the radius of the pipe ($kR \ll 1$):

$$f = \rho S(\omega - Uk)^2 w_0 \mathrm{e}^{\mathrm{i}(kx-\omega t)}. \tag{50}$$

The dispersion relation for the *slender* ($kR \ll 1$) fluid-conveying pipe finally writes,

$$D(k, \omega) = Bk^4 - m\omega^2 - \rho S(\omega - Uk)^2 = 0. \tag{51}$$

If one considers the deformation of a *slender* structure of any other cross section, with internal or external homogeneous potential flow, the fluid force

f is still of the form $f(x,t) = a(k)(\omega - Uk)^2 \mathrm{e}^{\mathrm{i}(kx-\omega t)}$, the function $a(k)$ being a characteristic function of the cross section geometry of the system. In the three-dimensional cases, the function a tends to a constant value A when $kR \to 0$, R being the characteristic dimension of the cross section. In the case of the fluid-conveying pipe, $a(k)$ can be deduced from equation (49) and $A = \rho S$. Other systems can be considered, giving different expressions for $a(k)$ and A, a 3D flag (Eloy et al., 2007), a 2D confined flag (Guo and Paidoussis, 2000), a 3D flag confined in the spanwise direction (Doaré et al., 2011), a cylinder with external flow (de Langre et al., 2007).

Instability of waves propagating in infinite 1D media: Local analysis We want now to perform a stability analysis of these media with respect to wave propagation. An infinite length medium is said to be stable if, for any sinusoidal wave of infinite extent in the x-direction and associated to a real wavenumber $k \in \mathbb{R}$, the corresponding frequencies given by $D(k,\omega) = 0$ are such that the displacement remains finite in time. The *local* instability criterion is then,

$$\text{Instability if } \exists\, k \in \mathbb{R} \setminus \mathrm{Im}[\omega(k)] > 0. \tag{52}$$

This approach is said to be *temporal*, since it consists of examining the *temporal* evolution of waves in time [1].

The behaviour of ω when k is varied is represented in Figure 11 for the plate and pipe cases and for different values of the flow velocity U. For both systems, as soon as the flow velocity is not zero, there exist a range $[0, k_c]$ of wavenumbers for which one corresponding frequency has a positive imaginary part. Consequently, these media bear unstable waves at any flow velocity. In fact decreasing or increasing the flow velocity do not change the stability properties, but has an effect on the characteristic wavelengths of the unstable waves. k_c increases as U increases; the higher is the velocity, the smaller is the smallest unstable wave. This will have practical consequences when we will study the stability of finite length systems. These aspects will

[1] If one is intersested in the response of the medium to localized disturbances, the *spatial* approach is more relevant. Conversely to the *temporal* approach it consists of the calculation of wavenumbers associated to one fequency. For plates or beams in presence of flows, the dispersion relation takes the form of a fourth-order polynomial in k in case of slender structures or more complicated forms in more general cases (see equation 49 for example). The response of unstable media to localized disturbances involves studies of the dispersion relation using the *spatial* approach in the complex $\omega-$ and $k-$ planes which are beyond the scope of the present lecture notes.

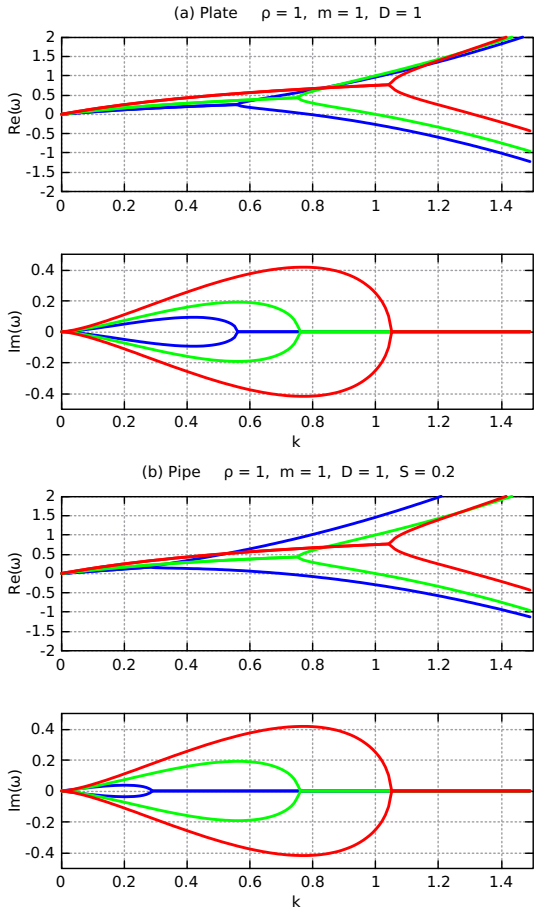

Figure 11. Real and imaginary parts of ω as function of k for different values of the flow velocity U (blue:0.7, green:1, red:1.5) in the plate and pipe cases.

be regarded in more details in section 2 at the same time we will address the influence of structural dissipation.

Unstable modes in finite length sysems: Global analysis The global analysis considers the same local medium, but in a finite domain $\Omega = [0, L]$, associated with a set of boundary conditions, denoted as $\mathcal{B}_i(y) = 0$, $i = 1...N$, where N is the maximal order of the spatial derivatives in the local equation. In the present elastic beam or plate problem, $N = 4$ and the boundary conditions are classical beam theory boundary conditions, which, among other, can be clamped,

$$w(x_0, t) = \left.\frac{\partial w}{\partial x}\right|_{(x_0,t)}, \tag{53}$$

pinned,

$$w(x_0, t) = \left.\frac{\partial^2 w}{\partial x^2}\right|_{(x_0,t)}, \tag{54}$$

or free,

$$\left.\frac{\partial^2 w}{\partial x^2}\right|_{(x_0,t)} = \left.\frac{\partial^3 w}{\partial x^3}\right|_{(x_0,t)}, \tag{55}$$

where $x_0 = 0$ or L is the location of the boundary condition.

The linear dynamics of this slender structure is governed by a wave equation of the form,

$$\frac{\partial^2}{\partial t^2}\mathcal{M}\left[w(x,t)\right] + \frac{\partial}{\partial t}\mathcal{C}\left[w(x,t)\right] + \mathcal{K}\left[w(x,t)\right] = 0 \quad \text{on } \Omega = [0, L], \tag{56}$$

where $\mathcal{M}$, $\mathcal{C}$ and $\mathcal{K}$ are mass, damping and stiffness operators respectively. In the fluid-conveying pipe case, their respective expression can be easilly recovered after equation (51):

$$\mathcal{M} = m + \rho S\,, \quad \mathcal{C} = \rho S U \frac{\partial}{\partial x} \quad \mathcal{K} = B\frac{\partial^4}{\partial x^4} + \rho S U^2 \frac{\partial^2}{\partial x^2}. \tag{57}$$

From now on, we will focus on the fluid-conveying pipe model system. Other systems such as plates, flags or cylinders in axial flow are governed by very similar equations and present very similar stability properties.

Considering ansatz solutions of the form $y = \phi(x)e^{-\mathrm{i}\omega t}$ and inserting this in equation (56), one obtains a Sturm-Liouville problem which solution is represented by an infinite set of eigenfunctions $\phi_n(x)$ and eigenfrequencies

$\omega_n{}^2$. The instability condition reads then:

$$\text{Instability if } \exists\, \omega_n \ \setminus \mathrm{Im}[\omega_n] > 0. \tag{58}$$

In most cases, numerical methods are necessary to solve this kind of problems. We present here a so-called Galerkin method to compute approximate solutions. The solution $w(x,t)$ is decomposed on a truncated function basis that satisfies the boundary conditions,

$$w(x,t) = \sum_{n=1}^{N} \phi_n(x) q(t). \tag{59}$$

In practice, a good choice of eigenfunctions can be a subset of operators in equation (56) with the same boundary conditions, for which an analytical solution exists. A natural choice for slender beams in flows are the eigenmodes of the same beam in vacuum. After defining a scalar product,

$$\langle f, g \rangle = \int_\Omega f g \mathrm{d}x, \tag{60}$$

the approximated form of w defined in equation (59) is introduced in (56), which is next projected on a mode $\phi_m(x)$. One finally obtains a discrete set of coupled oscillator equations,

$$M\ddot{\vec{q}} + C\dot{\vec{q}} + K\vec{q} = 0. \tag{61}$$

The coefficients of the matrices M, C, and K result from the projection of the inertia, damping and rigidity operators of equation (56),

$$M_{mn} = \langle \mathcal{M}(\phi_n), \phi_m \rangle \ , \quad C_{mn} = \langle \mathcal{C}(\phi_n), \phi_m \rangle \ , \quad K_{mn} = \langle \mathcal{K}(\phi_n), \phi_m \rangle. \tag{62}$$

Hence, one ends up with an approximate equivalent of the continuous, finite system, in the form of a finite degree of freedom mechanical system.

The discrete mechanical equations presented in section 1.1 and that obtained by Galerkin discretisations of equation (56) all fall into the category represented by the general discrete equation (61). The analysis of such systems is done by looking for solutions in the form of time-harmonic solutions of the form $\vec{q} = \vec{q}_0 \mathrm{e}^{-\mathrm{i}\omega t}$. This leads to a second order eigenvalue problem

[2] Note that most of the systems considered here are non self-adjoint. Hence, a complete solution set consists of a biorthogonal set of eigenfunctions and adjoint eigenfunctions. This has a practical importance when one wants to analyse the response of such non conservative problems to external forcings.

for the eigenfrequency. The criterion for global instability is then given by (58). If the studied discrete system comes from a Galerkin discretisation (section 1.4), the corresponding eigenvector represents the eigenmode in the form of a combination of functions $\phi_n(x)$.

Similarly to the discrete structures in flows presented in section 1.1, the fluid conveying pipe is prone to buckling or flutter instabilities, which are intrinsically related to the symmetries of matrices C and K. In particular, depending on the boundary conditions, the flow added stiffness term of equation (57) can contribute to symmetric or skew-symmetric parts in equations (61-62). This will be regarded in more details in the next section at the same time we consider the effect of damping on stability.

2 Damping induced instabilities of structures coupled to a flow

The effect of damping in the fluid-structure system is now addressed. It is a conventional linear damping, as opposed to the flow-induced damping evidenced in some cases of the previous section. It can be easily predicted that only one type of flow-induced instabilities can be eventually enhanced after introduction of damping:

- In the negative flow-induced damping instabilities, the conventional damping counteracts the flow effects and prevents instability.
- The negative flow-induced stiffness instability is a static instability that is not affected by velocity dependent forces.
- The skew-symmetric coupling in the stiffness matrix induces a dynamic instability that might be triggered earlier by the addition of damping. This is the case detailed hereafter.

Hence, wing flutter results will be presented. Next, the fluid conveying-pipe will be considered as a model problem of a continuous system that bears unstable waves, but also bears unstable modes when boundaries are added. This system will be used to travel from waves to modes, and next from modes to discrete oscillators and see the link between the local and global stability properties with respect to the dissipation-induced instabilities.

2.1 Damping induced instabilities of wings

The two degrees of freedom wing in flow has been introduced in section 1.3. It was shown that the flow couples the two degrees of freedom of the system. If this coupling is skew-symmetric, eigenfrequencies form complex conjugate pairs and induce an instability of the flutter type. The equations governing the dynamics of this system are identical to that of the Ziegler pendulum (Ziegler, 1952). It's stability is addressed in details in the chapter

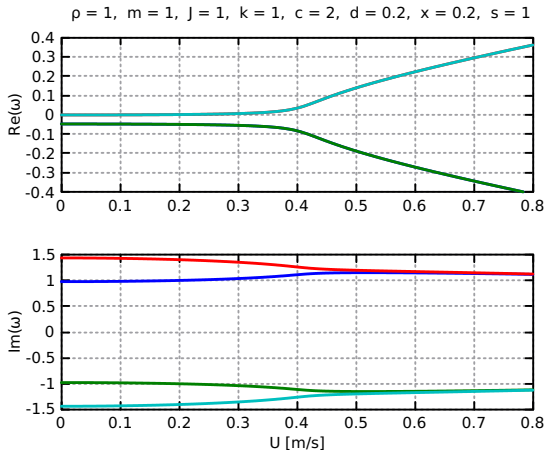

Figure 12. Evolution of ω as function of the flow velocity U for the two-DOF wing with added dissipation. Typical values of the other parameters are chosen.

written by Davide Bigoni. Mathematical aspects are developped in the chapter written by Oleg Kirillov. The damping induced instability of wings is hence only briefly presented here in a typical example.

Consider that a dissipative force is added to the system on the translation degree of freedom. A dissipation matrix is added to system, which now writes,

$$\begin{bmatrix} m & 0 \\ 0 & J \end{bmatrix} \begin{bmatrix} \ddot{y} \\ \ddot{\theta} \end{bmatrix} + \begin{bmatrix} \gamma & 0 \\ 0 & 0 \end{bmatrix} \begin{bmatrix} \dot{y} \\ \dot{\theta} \end{bmatrix} \tag{63}$$

$$+ \begin{bmatrix} k & kx - \frac{1}{2}\rho U^2 S C'_L \\ kx & c + kx^2 - \frac{1}{2}\rho U^2 S d C'_L \end{bmatrix} \begin{bmatrix} y \\ \theta \end{bmatrix} = \begin{bmatrix} 0 \\ 0 \end{bmatrix}. \tag{64}$$

As discussed in section 1.3, the instability is linked to the energy transfers between the flow and the structure, which is in turn related to the respective phases of translation and rotation. Adding damping modifies the relative phases of these degree of freedom an may hence have a destabilising effect. The evolution of the eigenfrequencies when the flow velocity is increased from zero is shown in Figure 12 for the same parameters as in Figure 7 with an additionnal damping $\gamma = 0.1$. The occurence of a positive imaginary part eigenfrequency is observed at a velocity $U \sim 0.18$ which is much lower than that of the case without dissipation, $U \sim 0.41$ (see section 1.3).

2.2 The fluid-conveying pipe model system

We consider again the dynamic equation of the pipe with internal flow presented in equations (56-57). As already mentionned, this is a simple and general equation describing the linear dynamics of a slender structure interacting with an axial flow. Many other systems share the exact same equations, provided typical lengthscales flexural deformations are large compared to the transverse dimensions of the structure (see discussion after equation 50). It consists of an Euler-Bernoulli beam with additional terms taking into account an internal flow of an inviscid fluid. It is written again here using capital letters for all the variables in order to allow a future non dimensionalisation of the equations,

$$B\frac{\partial^4 Y}{\partial X^4} + m\frac{\partial^2 Y}{\partial T^2} + \rho S\frac{\partial^2 Y}{\partial T^2} + \rho SU^2\frac{\partial^2 Y}{\partial X^2} + 2\rho SU\frac{\partial^2 Y}{\partial X \partial T} = 0 \tag{65}$$

The first two terms in this equation are the flexural rigidity and inertia terms of the linearized Euler-Bernoulli equation. The third term is an inertia term that comes from the presence of the fluid inside the pipe. The fourth term may be understood as a centrifugal term that arises as soon as the beam experiences a local curvature. Finally the fifth term is generally referred to as a Coriolis force and may be interpreted by considering a portion of the pipe moving at a constant velocity. Due to the presence of a moving mass inside, a force is exerted on this portion of the pipe when it rotates.

When damping is to be considered, one may add one or both of these two additional forces to the wave equation,

$$\mathcal{D}_f(Y) = C\frac{\partial Y}{\partial T}\ , \quad \mathcal{D}_s(Y) = B^*\frac{\partial^5 Y}{\partial X^4 \partial T}. \tag{66}$$

The first case is referred to as viscous damping and is generally a consequence of the presence of a viscous fluid at rest around the pipe. The second is called structural damping and is the consequence of a viscoelastic behavior of the material that constitutes the pipe.

After introducing the characteristic length $\eta = \left(\frac{B}{\rho SU^2}\right)^{1/2}$ and time $\tau = \left(\frac{(m+\rho S)\eta^4}{B}\right)^{1/2}$ and rescaling all dimensional quantities using these two parameters, the wave equation without dissipation takes a form that depends only on one independent parameter β,

$$\frac{\partial^2 y}{\partial t^2} + \frac{\partial^4 y}{\partial x^4} + \frac{\partial^2 y}{\partial x^2} + 2\sqrt{\beta}\frac{\partial^2 y}{\partial x \partial t} = 0, \tag{67}$$

where β is the mass ratio,

$$\beta = \frac{\rho S}{m + \rho S} \in [0, 1]. \tag{68}$$

Note that the case $\beta = 0$ is strictly equivalent to a cantilevered beam with a follower force, referred to as the Beck's column (Beck, 1952), which is a continuous equivalent to the Ziegler's pendulum (Ziegler, 1952). The opposite case $\beta = 1$ is strictly equivalent to the problem of travelling webs or chains (Asokanthan and Ariaratnam, 1994).

In their dimensionless forms, the terms operators now write,

$$d_f(y) = c\frac{\partial y}{\partial t} , \quad d_s(y) = \alpha\frac{\partial^5 y}{\partial x^4 \partial t}. \tag{69}$$

When considering a finite length system, the non-dimensional length has to be introduced,

$$l = \frac{L}{\eta} = UL\sqrt{\frac{\rho S}{B}}, \tag{70}$$

and two boundary conditions have to be specified at each boundary. They read

$$y(x = x_0, t) = y'(x = x_0, t) = 0 , \quad y''(x = x_0, t) = y'''(x = x_0, t) = 0, \tag{71}$$

for a clamped end and a free end respectively, where the primes $(.)'$ denote derivation with respect to x and x_0 takes the value 0 or l.

Local stability In our study of the stability properties of the fluid-conveying pipe system, let us first address the stability of waves in the infinite medium, an approach referred to as local. It directly follows from equation (67) that the dispersion relation of the undamped fluid-conveying pipe reads,

$$D(k, \omega) = k^4 - \omega^2 + k^2 + 2\sqrt{\beta}k\omega = 0. \tag{72}$$

The frequency associated to a real wavenumber k then reads,

$$\omega_\pm = \sqrt{\beta}k \pm k\sqrt{\beta + k^2 - 1}. \tag{73}$$

For $\beta \in [0, 1[$ and $k \in [0, \sqrt{1-\beta}]$, frequencies $\omega_\pm$ are complex conjugate and the positive imaginary part of one of them gives rise to a wave with an amplitude exponentially growing in time. For $k > \sqrt{1-\beta}$, $\omega(k) \in \mathbb{R}$ and

waves are said neutral. Thus the medium is locally unstable $\forall \beta \in [0, 1[$. Conversely for $\beta \geq 1$, the medium is neutrally stable[3].

In various studies on the effect of damping on wave propagation, the key role of the wave energy has been evidenced. Although introduced in the context of shear layer waves between two non miscible fluids (Cairns, 1979), the definition is generic and can be readily used in any mechanical system. Consider an harmonic wave with $\omega \in \mathbb{R}$ and $k \in \mathbb{R}$ and $D(k, \omega) = 0$. The wave energy E is defined as the work done on the system to establish this neutral wave from $t = -\infty$ to $t = 0$, and reads,

$$E = -\frac{\omega}{4} \frac{\partial D}{\partial \omega} y_0^2. \tag{74}$$

If E is negative, it means that energy has to be removed from the system to establish the wave. The latter is then referred to as a *Negative Energy Wave* (NEW) (von Laue, 1905).

Now consider that a small amount of viscous damping is added in the medium, so that the dispersion relation takes the form,

$$D_1(k, \omega + \delta\omega) = D(k, \omega + \delta\omega) - ic(\omega + \delta\omega) = 0, \tag{75}$$

where $\delta\omega \ll \omega$ is a small perturbation to the frequency introduced by the damping, which satisfies at order one,

$$\delta\omega \left. \frac{\partial D}{\partial \omega} \right|_{(k,\omega)} \simeq ic\omega. \tag{76}$$

We readily deduce from this expression the pertubation on the growth rate $\delta\sigma = \mathrm{Im}(\delta\omega)$,

$$\delta\sigma \simeq \frac{c\omega}{\partial D / \partial \omega}. \tag{77}$$

This quantity has the opposite sign of the wave energy E. A NEW is hence destabilized by viscous damping. The same calculation performed with viscoelastic damping gives:

$$\delta\sigma \simeq \frac{\alpha k^4 \omega}{\partial D / \partial \omega}, \tag{78}$$

which leads us to the same conclusions.

[3] However, it has to be noted that $\beta > 1$ has no physical meaning in the present context (see the definition of β in equation 68).

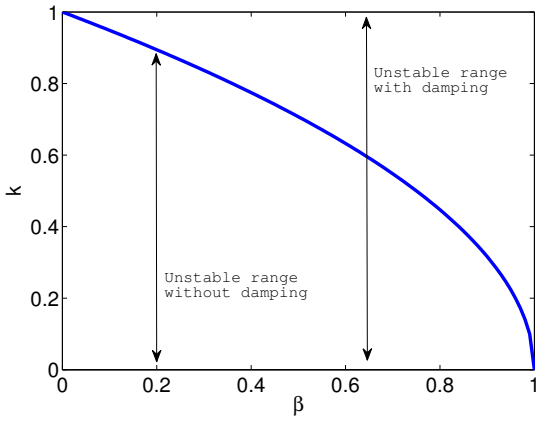

Figure 13. Range of unstable wavenumbers as function of β. This illustrates the fact that the range of wavenumbers $\sqrt{1-\beta}$ is stabilized by the Coriolis force and this range is then destabilized when damping is added in the medium.

In the fluid-conveying pipe case, the wave energy has for expression,

$$E_{\pm} = \frac{1}{2}k^2\sqrt{k^2+\beta-1}\left(\sqrt{k^2+\beta-1} \pm \sqrt{\beta}\right), \tag{79}$$

and E_- has negative values in the range $k \in]\sqrt{1-\beta}, 1[$. Hence, the range of temporally unstable waves becomes $[0, 1[$ when damping is added, whereas it was $k \in [0, \sqrt{1-\beta}]$ in the conservative case. Damping enlarged the range of unstable wavenumbers. Moreover, the system is now temporally unstable for any value of β, when it was for $\beta \in [0, 1[$ in the conservative case.

In Figure 13, the ranges of unstable wave in the damped and undamped cases are compared when the parameter β, quantifying the Coriolis force, varies from 0 to 1. It can be concluded from this figure that Coriolis force stabilizes waves, which are in turn destabilized by a small amount of damping. The same kind of behavior was observed in discrete gyroscopic systems by Thomson and Tait (1879).

Global stability Boundary conditions and finite length parameter l are now introduced. The dimensionless parameter l in equation (70) is proportional to both L and U, indicating that it can be seen as a dimensionless length or flow velocity. Although the limit $l = 0$ has no meaning when it is sought as a length, it can be achieved by letting the flow velocity vanish.

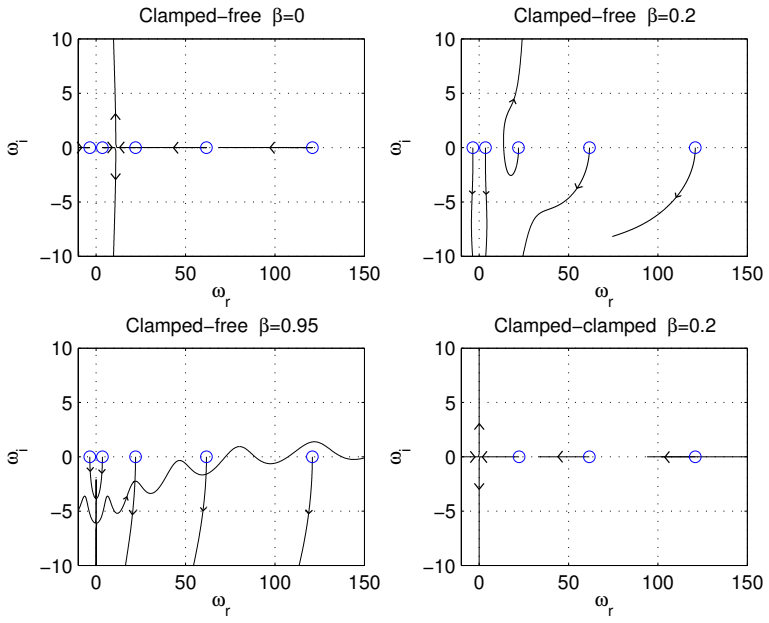

Figure 14. Evolution in the complex plane of the eigenfrequencies of the clamped-clamped and clamped-free pipe when the velocity parameter v is increased from zero, for different values of the mass ratio β.

In the finite length global approach, it is then more convenient to use L to rescale the lengths, so that the dimensionless wave equation becomes,

$$\frac{\partial^2 w}{\partial t^2} + \frac{\partial^4 w}{\partial x^4} + u^2 \frac{\partial^2 w}{\partial x^2} + 2\sqrt{\beta} u \frac{\partial^2 w}{\partial x \partial t} = 0, \tag{80}$$

where the length of the dimensionless problem is the unity and with,

$$u = l. \tag{81}$$

The Galerkin method presented in section 1.4 is used to obtain the results presented hereafter. The chosen test functions are the eigenmodes of the pipe without flow. The functions $\phi_n(x)$ are hence the eigenfunctions of equation (80) with the same set of boundary conditions and $u = 0$. These eigenfunctions are basically the eigenmodes of a beam and are known and well documented analytic functions (see for instance the book by Blevins

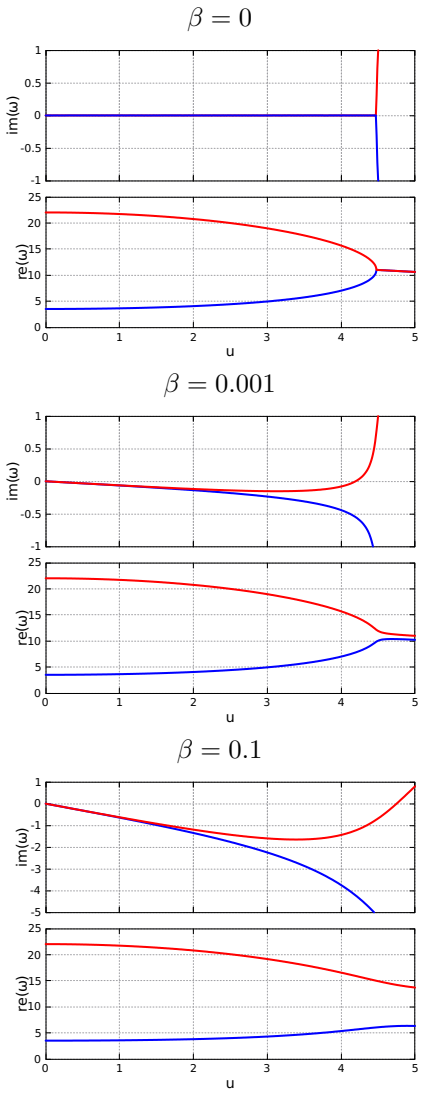

Figure 15. Real and imaginary parts of the two first eigenfrequency of the pipe as function of the non dimensional flow velocity u for 3 different values of β.

(Blevins, 1979)). Equation (80) is then projected on each mode ϕ_m, leading to N ordinary differential equations for the time variable, which read,

$$\ddot{\vec{q}} + 2\sqrt{\beta} v\, C\, \dot{\vec{q}} + (K + v^2 A)\vec{q} = 0, \tag{82}$$

where $\vec{q}$ is the vector containing modal displacments, as defined in equation (59). The coefficients of the matrices C, K and A result from the projection of the Coriolis, flexural stiffness and centrifugal operators respectively. Note that K is diagonal because the choosen test functions diagonalise the flexural stiffness operator $\frac{\partial^4}{\partial x^4}$. The coefficients of these matrices can be found in the litterature (Gregory and Païdoussis, 1966; Blevins, 1979; Païdoussis et al., 2011). They are reported in table 1 for two particular sets of boundary condition: clamped at both ends, and clamped uptream, free downstream. It is interesting to note here that the symmetries of the fluid-structure coupling matrices depend on the boundary conditions. In the clamped-clamped case, C is skew-symmetric and K_f is symmetric, while in the clamped-free case, C and K have both symmetric and skew-symmetric parts. This has consequences on the bifurcations properties of these two systems.

To illustrate the influence of the boundary conditions and the matrix symmetries, the evolution of the eigenfrequencies when v is increased from 0 is plotted in Figure 14 in four typical cases: a pipe clamped at both ends, a clamped-free pipe at $\beta = 0$, and a clamped-free pipe at $\beta = 0.2$ and $\beta = 0.95$. These graphs illustrate the typical behaviors of the eigenfrequencies when the flow velocity is increased. Different bifurcations are evidenced. In the case of a clamped-clamped pipe, instability always arises through a saddle-node bifurcation, also called pitchfork bifurcation. The instability is called static instability, or buckling. In the case of a clamped-free pipe, the bifurcation depends on the value of the mass ratio β. If $\beta = 0$, the dissipation matrix vanishes in equation (82) and the instability occurs via a Hopf bifurcation after the merging of two eigenfrequencies on the real axis. In the fluid-elastic community, this instability is referred to as flutter instability, as it results in self-sustained oscillations of the structure once the amplitude of the solution has been saturated by the nonlinear effects. When $\beta \neq 0$, the increase of the flow velocity has at first a stabilizing effect, related to the flow-induced damping (C matrix): all the eigenfrequencies travels towards the negative imaginary part half plane. When further increasing the flow velocity, one eigenfrequency changes its trajectory and crosses the real axis, giving rise to a flutter instability. The damping effect of the Coriolis force is further illustrated in Figure 15, where the evolution of the first two eigenfrequencies is plotted using a different representation as in Figure 14. For $\beta = 0$, it is clearly visible with both representations that the bifurcation occurs through a pinching of two eigenfrequencies on the real axis, and form

	Clamped-clamped	Clamped-free
C_{ii}	0	2
C_{ij}	$\frac{4\lambda_i^2\lambda_j^2}{\lambda_j^4-\lambda_i^4}\left[(-1)^{i+j}-1\right]$	$\frac{4}{(\lambda_i/\lambda_j)^2+(-1)^{i+j}}$
A_{ii}	$\lambda_i\sigma_i(2-\lambda_i\sigma_i)$	$\lambda_i\sigma_i(2-\lambda_i\sigma_i)$
A_{ij}	$\frac{4\lambda_i^2\lambda_j^2}{\lambda_j^4-\lambda_i^4}[\lambda_j\sigma_j-\lambda_i\sigma_i]\left[(-1)^{i+j}+1\right]$	$\frac{4(\lambda_i\sigma_i-\lambda_j\sigma_j)}{(\lambda_i/\lambda_j)^2+(-1)^{i+j}}$
λ_i	4.73004, 7.85320, 10.99560, 14.13717, 17.27876, $(2i+1)\frac{\pi}{2}$ for $i>5$	1.87510, 4.59091, 7.85476, 10.99554, 14.13717, $(2i-1)\frac{\pi}{2}$ for $i>5$
σ_i	0.982502, 1.000777, 0.999966, 1.000001, 1 for $i>4$	0.73, 1.018, 0.9992, 1.00003,0.99999, 1 for $i>5$

Table 1. Coefficients of the added damping matrix C and the added stiffness matrix A of equation (82). More details on these coefficients, for various sets of boundary conditions can be found in the reference book of Blevins (Blevins, 1979).

a complex conjugate pair after the bifurcation. When $\beta > 0$, Figure 14 shows that the instability occurs when a single eigenfrequency crosses the real axis. Figure 15 indicates that the eigenfrequencies are still approaching but their trajectories are deformed and they never form a dooble-root pair at the occurence of the instability.

Let us now address the effect of dissipation on the marginal stability of the clamped-free pipe. The global stability of the system is now characterized by plotting in the (β, l) plane the marginal stability curve in Figure 16a for $c = 0$ (no damping). This curve corresponds to the line in the (β, l) plane where the maximum growth rate $\max_n[\mathrm{Im}(\omega_n)] = 0$. In the same figure, the local stability criterion $\beta = 1$ is plotted. It appears then that the long system limit for global instability is the local stability criterion. In Figure 16b, different values of the dimensionless damping c from 0 to 1000 are

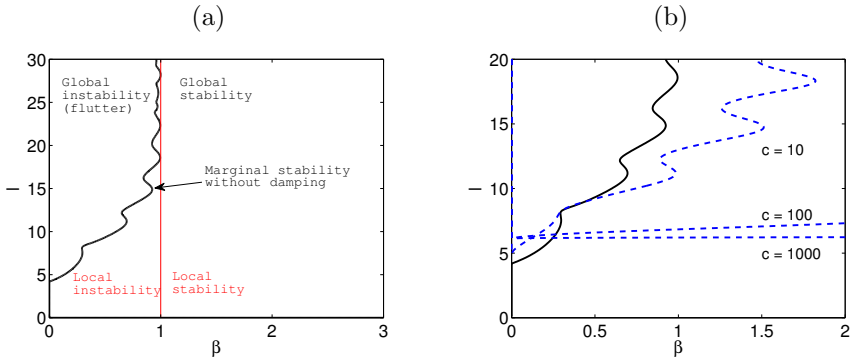

Figure 16. (a) Marginal global stability curve of the pipe conveying fluid in the parameter plane (β, l) (thick black) compared with the local stability criterion; (b) Marginal global stability curves for increasing viscous damping.

considered. The resulting marginal stability curves move continuously from the undamped limit to an horizontal limit. For $\beta \in [0, 0.2]$, the damping appears to have a stabilizing effect while it has a destabilizing effect for $\beta > 0.2$. Hence also for the finite length clamped-free pipe, damping can have a destabilizing effect. While in absense of damping, the global instability criterion of the finite length tends to the local one when l is increased, no such limit can be observed in the damped case because the damped medium is locally unstable $\forall \beta$. However, the horizontal limit observed at high values of the damping cannot be predicted by a local criterion, as addressed in the next section.

Lengthscale criterion We have discussed the emergence of instabilities and their dependence on the boundary conditions, through the matrix symmetries. We want here to show that provided we know the system can be destabilised by flutter, a simple lengthscale criterion can be invoked to predict the critical instability parameter. Firstly, let us note that in Figure 16a, for the values of the parameters comprised between the local and global stability curves, and below the dashed lines in Figure 16b the system is globally stable although locally unstable. In this situation, the confinement induced by considering a short system has for consequence to prevent unstable waves to play a role in the dynamics. This confinement effect can be quantified and can give an approximate criterion of stability. Let us state that an unstable wave can give rise to an unstable mode of the finite system

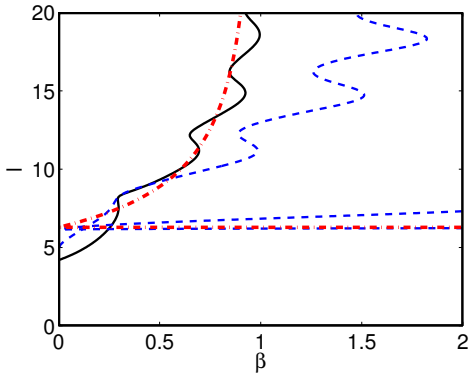

Figure 17. Global stability curves of the pipe conveying fluid in the (β, l) plane for increasing values of the viscous damping (plain and dashed lines), compared with the length criteria defined in equation (83) (dash-dotted lines).

only if its wavelength is smaller that the length of the system. The smallest unstable wavelengths are,

$$\lambda = \frac{2\pi}{\sqrt{1-\beta}}\,, \quad \lambda_d = 2\pi, \tag{83}$$

in the undamped and damped cases respectively. Plotted against the marginal stability curves in Figure 17, these criteria show a good agreement. The marginal stability curve goes continuously from the length criterion without damping to that with damping.

2.3 Conclusion

This section and the previous one were devoted to the description of flow-induced instabilities and the effect of dissipation on these instabilities. Cases of destabilization by dissipation have been identified for the 2-DOF wing system and the fluid-conveying pipe: in some particular ranges of the parameters, a stable system without dissipation can become unstable by the addition of a small amount of dissipation. For both systems, the key ingredient is the existence of non conservative fluid forces which induce skew-symmetric components in the stiffness matrix. In the fluid-conveying pipe system, we also identified a phenomenon of gyroscopic restabilization, which was cancelled by the addition of damping in the system.

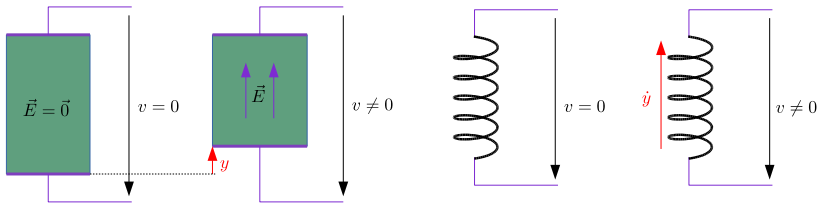

Figure 18. Sketch of two generic electromechanical converters. On the left, a piezoelectric material is deformed, which creates an electric field in the material. The presence of electrodes on the opposite faces generates a voltage. For small deformations, this voltage is proportionnal to the dispalcement that induced the deformation. On the right, a coil is moving at a velocity $\dot{y}$ in a magnetic field. This generates a voltage proportionnal to the velocity in the neighbour of an equilibrium position.

In the next section, we will consider that the dissipation comes from a mechanical to electrical energy transfer.

3 Applications in energy harvesting

In recent years, the use of flow-induced vibrations to harvest kinetic energy from environnemental flows has been the focus of a incrediblely large amount of scientific papers. Although the engineering interest and applicability in terms of economic or durabillity are still open questions, the concepts have raised numerous of intersting fundamental questions that are still open: what efficiency can we theoretically expect from these designs? How to optimize this efficiency? For a particular design or at a particular scale is piezoelectricity or induction the more efficient electromechanical coupling?

In this section, the basic modelling of flow-induced vibrations coupled to energy harvesting circuits is presented. Linear stability is addressed as well as non linear saturation of the instabilities.

3.1 Energy converters

The idea behind any energy converter is to convert a mechanical work into an electrical work. Two generic electromechanical converters are sketched on Figure 18. The first one consists of a piezoelectric material that is stretched or compressed consecutively to the displacement y of one of its boundaries. Due to its particular cristallographic arrangement, deformation

induces an electric field that can be converted as an electric voltage v if electrodes are placed on its boundaries. A second electromechanical converter that can be considered is based on the electromagnetic induction. A coil moving at a velocity $\dot{y}$ can generate a voltage at its outlets if it moves in a magnetic field.

3.2 Models of energy harvesting systems based on flow-induced vibrations

In order to introduce the principles of flow-induced vibrations based energy harvesters, we will consider here a simple system that becomes unstable by negative added damping. The system and the den Artog criterion for instability are presented in section 1.2. Equation (8) describing the dynamics of this system can be simplified to

$$m\ddot{y} + (c_d + AU)\dot{y} + ky = 0, \tag{84}$$

where A is an aerodynamic coefficient depending on the profile geometry and its reference position (the equilibrium position around which there may exist an oscillation). If A is negative, there is a possibility of negative damping once a critical velocity is reached, hence exponentially growing oscillations may appear.

The coupled systems are sketched on Figure 19 where an energy harvesting device is added to the mechanical system studied in section 1.2. If it consists of a piezoelectric element, it behaves electrically as a voltage generator in series with a capacitive device. The charge displacement q in the piezoelectric device reads

$$q = \chi y + Cv, \tag{85}$$

where χ is a coupling coefficient which depends on the material, its cristallographic properties, and the geometry. If the converter consists of a coil in a magnetic field, it behaves electrically as a voltage generator in series with an inductance[4]. The charge displacement in the coil satisfies,

$$L\ddot{q} + \chi\dot{y} = v. \tag{86}$$

The coupling coefficient χ here depends on the magnetic field, the coil geometry and the direction of the displacement.

We have hence modelled the so-called direct effect, which concerns the coupling from the mechanical part to the electrical part. The converse effect

[4]In practice, the coil has also a DC-resistance, but it is neglected in this introductory approach.

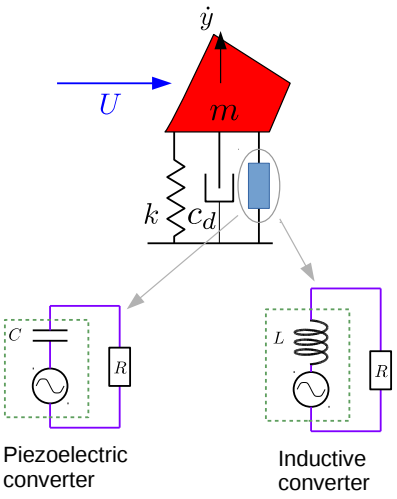

Figure 19. Top: an energy harvesting device based on the vibrations generated by negative flow-induced damping. Bottom: electrical circuits of the piezoelectric and inductive energy converted coupled to a resistance modelling the energy harvesting.

is also present. A voltage applied at the outlets of the piezoelectric material induces a force on the device,

$$F = -\chi v. \tag{87}$$

Similarly, a current in the coil induces a force on itself,

$$F = L\chi\dot{q}. \tag{88}$$

These electrical devices are connected to a resistance R modelling the energy harvesting, as sketched in Figure 19. Making use of the Ohm's law we can provide an additionnal constitutive relation to the electrical model:

$$v + R\dot{q} = 0. \tag{89}$$

Linear models

Using equations (84,85,87,89), one obtains a set of coupled linear equations modelling the dynamics of the profile coupled with an electrical circuit

through piezoelectric coupling,

$$m\ddot{y} + (c_d + AU)\dot{y} + \left(k + \frac{\chi^2}{C}\right) y + \frac{\chi}{C} q = 0, \tag{90}$$

$$R\dot{q} + \frac{1}{C} q + \frac{\chi}{C} y = 0. \tag{91}$$

Equation (90) can be seen as a damped oscillator equation coupled to the electrical part through the term $(\chi/C)q$ while equation (91) is the dynamical equation of an RC circuit coupled to the mechanical part through the term $(\chi/C)y$. Hence, piezoelectricity couples the dynamics of the mechanical system and the electrical circuit through two symmetrical terms involving structural and charge displacements. Additionnally, the fact that electrical energy can be stored in the equivalent capacity induces an additionnal stiffness χ^2/C in the structural dynamics part.

In the same manner, using equations (84,86,88,89), the dynamical system modelling the dynamics of the profile coupled with an electrical circuit through inductive coupling takes the form

$$m\ddot{y} + (c_d + AU)\dot{y} + ky - \chi\dot{q} = 0, \tag{92}$$

$$L\ddot{q} + R\dot{q} + \chi\dot{y} = 0. \tag{93}$$

Here, the mechanical oscillator equation is coupled to the electrical part through a term propotionnal to $\dot{q}$ and the dynamical equation of an LC circuit is symmetrically coupled to the mechanical part through a term proportionnal to $\dot{y}$.

Let us first analyse the linear dynamics and stability of piezoelectric energy harvester. In order to simplify the parametric analysis, the equations will be put in non dimensionnal form. The following dimensionless variables are introduced:

$$\bar{t} = t\sqrt{\frac{k}{m}}\,, \quad \bar{y} = \frac{y}{D}\,, \quad \bar{q} = q\frac{1}{\sqrt{kC}D}, \tag{94}$$

where D is a characteristic length of the system[5]. The dimensionless set of equations, equivalent to equations (90-91) is then obtained as,

$$\ddot{\bar{y}} + (\gamma - \delta)\dot{\bar{y}} + (1 + \alpha^2)\bar{y} + \alpha\bar{q} = 0, \tag{95}$$

$$\beta\dot{\bar{q}} + \bar{q} + \alpha\bar{y} = 0, \tag{96}$$

[5]It can be a typical length of the cross section profile for instance. But in this context, the choice of the length as no incidence on the results of the analysis

with

$$\alpha = \frac{\chi}{\sqrt{kC}}\ , \quad \beta = RC\sqrt{\frac{k}{m}}\ , \quad \gamma = \frac{c_d}{\sqrt{km}}\ , \quad \delta = -\frac{AU}{\sqrt{km}}. \tag{97}$$

α is the piezoelectric coefficient. β is the ratio between the electrical timscale RC and the mechanical timescale $\sqrt{\frac{k}{m}}$. γ is the dimensionless structural damping and δ can be sought as the dimensionless flow velocity.

In order to study the linear dynamics of the system, it is written in martix form, at order one for the time derivatives:

$$\begin{bmatrix} 1 & 0 & 0 \\ 0 & 1 & 0 \\ 0 & 0 & \beta \end{bmatrix} \begin{bmatrix} \dot{y} \\ \ddot{y} \\ \dot{q} \end{bmatrix} + \begin{bmatrix} 0 & -1 & 0 \\ 1+\alpha^2 & \gamma - \delta & \alpha \\ \alpha & 0 & 1 \end{bmatrix} \begin{bmatrix} y \\ \dot{y} \\ q \end{bmatrix} = 0 \tag{98}$$

Looking for solutions in the form

$$\begin{bmatrix} y \\ \dot{y} \\ q \end{bmatrix} = \vec{V}\mathrm{e}^{\lambda t} = \vec{V}\mathrm{e}^{\lambda_r t}\mathrm{e}^{\mathrm{i}\lambda_i t}, \tag{99}$$

one obtains an eigenvalue problem of the form $\lambda\vec{V} = -M_1^{-1}M_2\vec{V}$, where M_1 and M_2 are the first and second matrices of equation (98) respectively. The real and imaginary parts of the eigenvalues are plotted as function of the dimensionless velocity δ in Figure 20 for $\alpha = 0$ (no piezoelectric coupling) and $\alpha = .75$ for typical values of the other parameters. For $\alpha = 0$, the eigenvalues are that of two uncoupled systems:

- A mechanical oscillator. Two of the three eigenvalues belong the the oscillator dynamics. They are complex conjugate. Their imaginary part correspond to the circular frequency of the oscillations (see equation 99), while their real part correspond to the growth rate. A positive real part leads to exponentially growing oscillations (instability). In the particular case of the plot, the critical value δ_{crit} for instability is $\sim .1$.
- An RC circuit. One real negative eigenvalue is found. Its value is the inverse of the characteristic time decrement of a capacity discharging in a resistance.

When piezoelectric coupling is added to the system, one can make the following observations.

- The imaginary part of the eigenvalues of the mechanical part increases. The additionnal stiffness induced by the energy stored in the capacity (α^2 term in equation 95) increases the frequency of the oscillations.

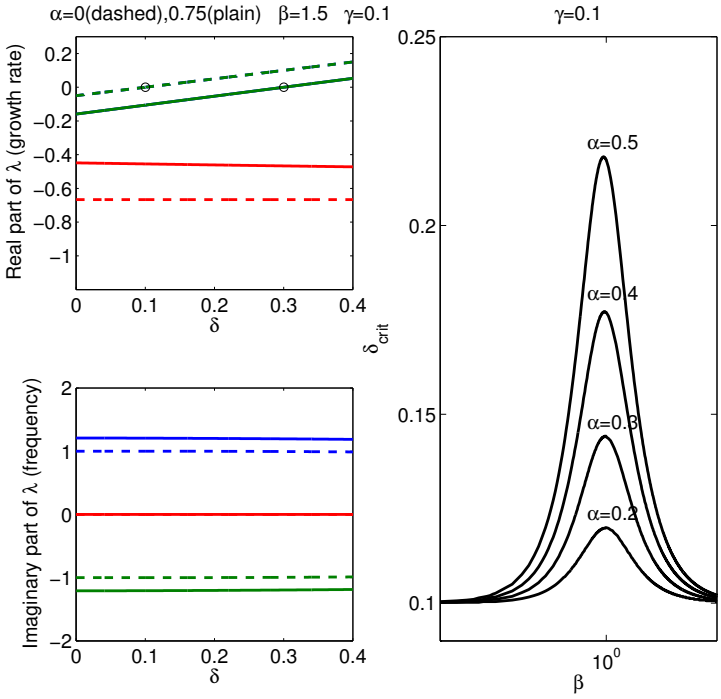

Figure 20. Galloping system of figure (19) with a piezoelectric energy harvester. Left: Real and imaginary parts of λ as function of the dimensionless velocity δ. The circles are a guide for the eyes indicating the crossing of the curve with the horizontal axis. Right: critical value of the dimensionless velocity δ as function of the timescale ratio β.

- Damping induced by the energy dissipation in the resistance increases the apparent damping seen by the mechanical oscillator. It hence increases the criticical velocity δ_{crit}.
- The dynamics of the electrical circuit is influenced by the mechanical part. The characteristic time hence varies with δ.

In the right plot of Figure 20 the value of δ_{crit} is plotted as function of β for different values of α. It appears on this plot that the critical velocity equals $\sim .1$ for small and large values of β. If β is sought as the dimensionless resitance, small values corresponds to a closed circuit. In this situation, the voltage is cancelled and the force induced by the reverse piezoelectric effect vanishes. The opposite case of large β (or large resistance) corresponds to an open circuit. Here, there is no charge displacement in the circuit which do not dissipate any energy in the resistance. There is no additional induced damping and the critical velocity is not modified by piezoelectric coupling. However, there is a voltage at the outlets of the piezoelectric material, and the additionnal stiffness term still exists. Between these two limit cases, the influence of piezoelectric coupling is maximized around $\beta = 1$. For this value of β, the electrical circuit synchronizes with the mechanical system. This gives us a condition for maximizing the influence of the electrical part on the mechanical part: *synchronization*.

The same analysis can be performed with an energy haverster of the inductive type. The electrical charge displacement is now non dimensionalized using

$$\bar{q} = q\frac{1}{D}\sqrt{\frac{L}{m}}, \tag{100}$$

while the characteristic time and displacement used for non dimensionalization are the same as in the piezoelectric case. One can finally write the dimensionless dynamical equations as,

$$\ddot{\bar{y}} + (\gamma - \delta)\dot{\bar{y}} + \bar{y} - \alpha\dot{\bar{q}} = 0, \tag{101}$$

$$\ddot{\bar{q}} + \frac{1}{\beta}\dot{\bar{q}} + \alpha\dot{\bar{y}} = 0, \tag{102}$$

with

$$\alpha = \frac{\chi}{\sqrt{kL}}\ , \quad \beta = \frac{L}{R}\sqrt{\frac{k}{m}}, \tag{103}$$

and γ and δ unchanged.

In the same manner as in the case of piezoelectric coupling, this linear system can be written at order one for the time derivatives. The system

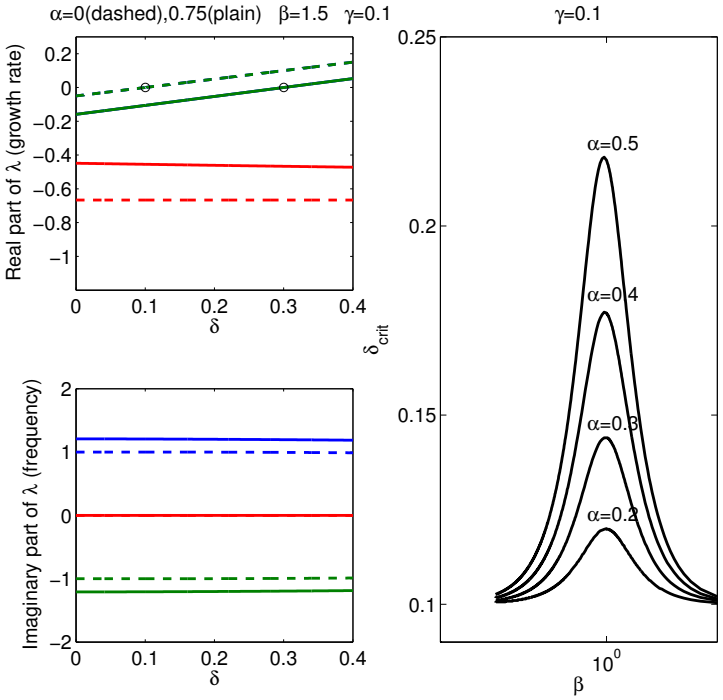

Figure 21. Galloping system of figure (19) with an inductive energy harvester. Left: Real and imaginary parts of λ as function of the dimensionless velocity δ. Right: critical value of the dimensionless velocity δ as function of the timescale ratio β.

writes then

$$\begin{bmatrix} 1 & 0 & 0 \\ 0 & 1 & 0 \\ 0 & 0 & 1 \end{bmatrix} \begin{bmatrix} \dot{y} \\ \ddot{y} \\ \ddot{q} \end{bmatrix} + \begin{bmatrix} 0 & -1 & 0 \\ 1 & \gamma - \delta & -\alpha \\ 0 & \alpha & 1/\beta \end{bmatrix} \begin{bmatrix} y \\ \dot{y} \\ \dot{q} \end{bmatrix} = 0 \qquad (104)$$

The stability analysis is again performed through an eigenvalue analysis. Typical results are plotted on Figure 21. It is remakable here that the stability results are almost identical in the inductive coupling case. All the most salient features evidenced in the piezoelectric case can also be evidenced in the inductive case.

Non linear saturation and efficiency

The linear system presented in the previous section still needs some improvement to satisfactorly model a real energy harvesting system. Indeed, when an instability is evidenced, the model predicts exponential growth of the oscillations. Of course, oscillations in real systems never grow to infinity. Instead, the system reach a saturated regime at a finite amplitude, caused by non linear forces that start to play a role when amplitudes reach finite values. These forces may originate from aerodynamic effects at large oscillation amplitudes, non linear material behaviour or structural geometrical non linearities. In the present approach, this will be modelled using a non linear cubic damping. A force $f_n l$ is then added on the right side the dynamics of the mechanical system:

$$f_{nl} = -k_{nl}\dot{x}^3. \tag{105}$$

This non linear stifness can be seen as a low order approximation of non linearities present in the system, or in other words, as the term of a Taylor expansion of the force next to the linear term. The resulting non linear system can then be integrated in time for a given set of parameters and initial conditions, using any numerical method. If the parameters are such that the system is linearly unstable, its dynamics consists of an oscillation with exponentially growing amplitude as long as amplitude is small and nonlinear terms are negligible. At larger amplitude, nonlinearities start to play a role in the dynamics and amplitude saturate. This is illustrated in the top graph of Figure 22a for a typical set of parameters. On this graph, cases $\alpha = 0$ (no piezoelectric coupling) and $\alpha = 0.3$ are presented. It is visible that the coupling between the mechanical system and the energy harvesting circuit induce additionnal damping in the system that reduce the growth rate as well as the displacement amplitude in the saturated regime.

Now that the system once instability is triggered is able to saturate, we are interseted in the power transfered to the electrical circuit. The instantaneous power of heat conversion in the resistance, modelling energy harvesting is $P = R\dot{q}^2$, or in dimensionless form,

$$p = \beta\dot{\tilde{q}}^2. \tag{106}$$

This quantity is plotted as function of time in the bottom graph of Figure 22a. In the saturated regime, the power fluctuates between zero and a maximum value p_{max} with a period half of the mechanical oscillation period.

On Figure 22b, the amplitude of oscillation and p_{max} are ploted as function of the value of β. For each explored value of β, one nonlinear integration is performed until a limit cycle is obtained. This graph shows that for values of β around unity, synchronization enhance energy transfer from the

oscillating structure to the harvesting circuit: the vibration amplitude is lowered and at the same time, p_{max} is maximized.

Hence, synchronization between the mechanical oscillatons and the electrical conversion circuit are also found to enhance the energy transfer.

3.3 Conclusion

In this section, some basic concepts of energy harvesting from flow induced instabilities have been introduced with the help of a simple galloping system. We have in particular shown that the key parameter for an efficient energy transfer is synchronization fluid-solid dynamics with the electrical circuit, whtever the electromechanical coupling is, inductive or piezoelectric. Of course, when a practical design has to be realized, the question of synchronization can become a different challenge if one use induction or piezoelectric coupling.

The concepts introduced here with a very simple system of a galloping oscillator could be readily applied to other systems such as 2-DOF fluttering wing profiles, fluttering flags or pipes. As well as with classical dissipation, energy harvesting-induced dissipation can destabilize the system. Also, more sophisticated circuits can be considered. For instance, by adding an indutance in the piezoelectric energy harvester, one creates a resonant circuit that can improve the harvested power.

Bibliography

J.J. Allen and A.J. Smits. Energy harvesting eel. *Journal of fluids and structures*, 15:629–640, 2001.

S. F. Asokanthan and S. T. Ariaratnam. Flexural Instabilities in Axially oving Bands. *Journal of vibration and acoustics*, 116:275, 1994.

A. Barrero-Gil, G. Alonso, and A. Sanz-Andres. Energy harvesting from transverse galloping. *Journal of Sound and Vibration*, 329(14):2873–2883, 2010.

Y. Bazilevs, K. Takizawa, and T. E. Tezduyar. *Computational fluid-structure interaction: methods and applications*. John Wiley & Sons, 2013.

M. Beck. Die Knicklast des einseitig eingespannten tangential gedruckten stabes. *Z. Angew. Math. Phys.*, 3:225–229, 1952.

K. Y. Billah and R. H. Scanlan. Resonance, Tacoma Narrows bridge failure, and undergraduate physics textbooks. *American Journal of Physics*, 59 (2):118–124, 1991.

R. D. Blevins. *Formulas for natural frequency and mode shape*. Von Nostrand Reinhold, 1979.

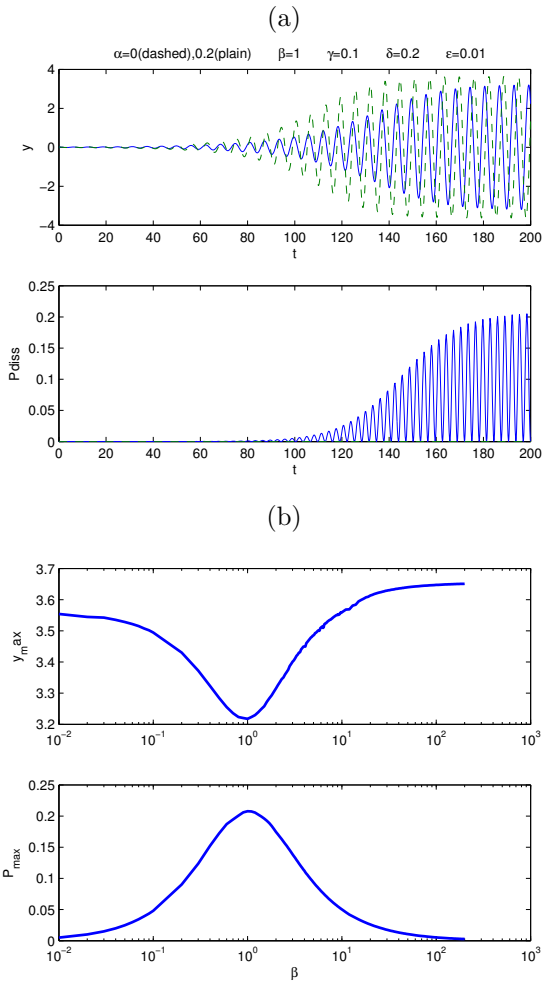

Figure 22. (a) Displacement (top) and instantaneous dissipated power in the resistance (bottom) as function of time for typical values of the dimensionless parameters. (b) In the saturated regime, maximum displacement (top) and maximum dissipated power for different values of β in the range $[10^{-2}, 2 \times 10^2]$.

R.D. Blevins. *Flow-induced vibration*. 1990.

R. A. Cairns. The role of negative energy waves in some instabilities of parallel flows. *Journal of Fluid Mechanics*, 92:1–14, 1979.

E. De Langre. Effects of wind on plants. *Annu. Rev. Fluid Mech.*, 40: 141–168, 2008.

E. de Langre, M. P. Païdoussis, O. Doaré, and Y. Modarres-Sadeghi. Flutter of long flexible cylinders in axial flow. *Journal of Fluid Mechanics*, 571: 371–389, 2007.

O. Doaré and S. Michelin. Piezoelectric coupling in energy-harvesting fluttering flexible plates: linear stability analysis and conversion efficiency. *Journal of Fluids and Structures*, 27(8):1357–1375, 2011.

O. Doaré, M. Sauzade, and C. Eloy. Flutter of an elastic plate in a channel flow: Confinement and finite-size effects. *Journal of Fluids and Structures*, 27(1):76–88, 2011.

E. H. Dowell, E. F. Crawley, H. C. Curtiss Jr, D. A. Peters, R. H. Scanlan, and F. Sisto. *A Modern Course in Aeroelasticity*. Kluwer Academic Publishers, Dordrecht / Boston / London, 1995.

C. Eloy, C. Souilliez, and L. Schouveiler. Flutter of a rectangular plate. *Journal of Fluids and Structures*, 23(6):904–919, 2007.

F. Gosselin and E. de Langre. Destabilising effects of plant flexibility in air and aquatic vegetation canopy flows . *European Journal of Mechanics - B/Fluids* , 28(2):271–282, 2009.

R. W. Gregory and M. P. Païdoussis. Unstable oscillation of tubular cantilevers conveying fluids. I. Theory. *Proceedings of the Royal Society of London*, A 293:512–527, 1966.

C. Q. Guo and M. P. Paidoussis. Stability of Rectangular Plates With Free Side-Edges in Two-Dimensional Inviscid Channel Flow. *Journal of Applied Mechanics*, 67(1):171–176, 2000.

M. P. Païdoussis. *Fluid-structure Interactions. Slender Structures and Axial Flow*, volume 2. Academic Press, 2004.

M. P. Païdoussis, S. J. Price, and E. de Langre. *Fluid-Structure Interactions - Cross-Flow-Induced Instabilities*. 2011.

L. Tang and M. P. Païdoussis. The coupled dynamics of two cantilevered flexible plates in axial flow. *Journal of Sound and Vibration*, 323(3-5): 790–801, 2009.

G.W. Taylor, J.R. Burns, Kammann S.M., Powers W.B., and T.R. Welsh. The Energy Harvesting Eel: A Small Subsurface Ocean/River Power Generator. *IEEE Journal of Oceanic Engineering*, 26(4):539–547, 2001.

Theodore Theodorsen. General theory of aerodynamic instability and the mechanism of flutter. Technical report, NASA, 1979.

W. Thomson and P. G. Tait. *Treatise on Natural Philosophy*. Cambridge University Press, 1879.

M. von Laue. The Propagation of Radiation in Dispersive and Absorbing Media. *Ann. Physik*, 1905.

H. Ziegler. Die stabilitätskrieterien der elastomechanik. *Ing.-Arch*, 20:49–56, 1952.